Theory of photopyroelectric spectroscopy of solids

Andreas Mandelis and Martin M. Zver
Photoacoustics Laboratory, Department of Mechanical Engineering, University of Toronto, Toronto, Ontario, M5S 1A4, Canada

(Received 25 June 1984; accepted for publication 4 October 1984)

Light absorption by a solid material and conversion of part, or all, of the optical energy into heat due to nonradiative deexcitation processes within the solid can give rise to an electrical signal in a pyroelectric thin film in contact with the sample. This effect forms the basis of a new spectroscopic technique for the study of condensed phase matter. A one-dimensional theory is presented, which describes the dependence of the pyroelectric signal on the optical, thermal, and geometric parameters of the solid/pyroelectric system. Specifically, the theory examines the conditions under which the photopyroelectric signal exhibits a linear dependence on the optical absorption coefficient of the solid. Thus a theoretical basis for the technique of photopyroelectric spectroscopy is established. Qualitative comparisons between predictions of the theory and preliminary experimental observations are used to test the applicability of the theory to experimental configurations of practical interest.

I. INTRODUCTION

The pyroelectric effect consists in the induction of spontaneous, rapid polarization in a noncentrosymmetric, piezoelectric crystal as a result of a temperature change in the crystal. Measurements of the pyroelectric effect first appeared shortly before World War I.[1–3] The use of pyroelectric detectors for the detection of infrared radiation was suggested early by Yeou[4] and Chynoweth[5]; however, practical pyroelectric detectors have been developed only recently.[6,7] Historically, the search for pyroelectric materials has been focussed on their infrared radiation detectivity[8,9] and their efficient high frequency responsivity.[7,10]

Very recently Coufal[11] and Mandelis[12] used thin pyroelectric polyvinylidene difluoride (PVDF or PVF_2) films to obtain pulsed laser and low modulation frequency spectra of various solid films and samples in contact with the pyroelectric transducer. These applications demonstrated the possibility of a new spectroscopic technique using pyroelectric thin films to detect optical absorption, nonradiative relaxation, and energy conversion processes in condensed phase matter. The experiments by Coufal[11] showed a detector response time of less than 100 ns for pulsed laser excitation, and high sensitivity in the spectroscopic detection of thin ($8.5 \pm 0.1\ \mu$m) films of Nd_2O_3 in poly(methyl methacrylate) (PMMA) at low light modulation frequency (5 Hz). The fast detector rise time in the above time-domain experiments is much more suitable for studies of transient phenomena than conventional microphone-coupled photoacoustic spectroscopy (PAS). Comparison between the pyroelectric and the piezoelectric PAS detection showed that both spectroscopic techniques have similar sensitivities and response times.[11] Coufal suggested that pyroelectric detection has distinct advantages over piezoelectric PAS, such as simplicity of calibration, insensitivity to acoustic noise and mechanical resonances, a high potential for signal-to-noise ratio improvement, and a flat response in the range 10^{-1}–10^{7} K/s.

The experiments by Mandelis[12] were aimed at characterizing the response of a photopyroelectric sample cell to an exciting light beam of variable wavelength and modulation frequency. The pyroelectric cell was shown to have a linear frequency response between 10 Hz and 2 kHz, a distinct advantage over the nonlinearities due to Helmholtz resonances present in commercially available microphone-coupled PAS cells. Mandelis further performed pyroelectric spectroscopic studies of Ho_2O_3 hydrated powders, kinetic studies of the chemical reduction of CuO into metallic copper by diluted HCl, and depth-profiling, frequency-domain studies of thin metallic copper plates.[12] The above experiments suggested the high potential for the use of pyroelectric thin film detectors for optical evaluation of materials and optical process studies. The main advantages of the technique were thus found to be its extreme simplicity, sensitivity, *in-situ* nondestructive probing ability, and adaptability to practical restrictions imposed by experimental system requirements.

While performing spectroscopic pyroelectric (photopyroelectric) studies of Ho_2O_3 powders, Mandelis observed inversion of the spectral features of the pyroelectric signal amplitude at a high modulation frequency (50 Hz), with no respective changes of the photopyroelectric phase. These seemingly surprising phenomena, together with the distinct experimental advantages and the promise of the above technique suggest the need for a theoretical foundation to understand and exploit those system properties which are responsible for the spectroscopic capability of the technique.

This paper is concerned with a one-dimensional photopyroelectric model of a solid sample in intimate contact with a pyroelectric thin film, and supported by a nonabsorbing backing material in an open cell. The emphasis is placed on the conditions and/or restrictions imposed on the values of system parameters, by the theory so that the described technique can produce spectroscopic signals linear in the optical absorption coefficient of the material under examination. Thus, the limits of validity of photopyroelectric spectroscopy as a spectroscopic technique are identified. The formalism allows for the practical consideration of a finite optical absorption coefficient for the pyroelectric detector, the value

 0021-8979/85/094421-10$02.40

of which depends, at a given light source wavelength, on the optical coating deposited on the surfaces of the detector by the manufacturer (e.g., nickel[13]).

II. MODEL

A one-dimensional geometry of a photopyroelectric system is shown in Fig. 1. A solid sample, of thickness L_s, is irradiated by monochromatic light of wavelength λ, whose intensity is modulated at angular frequency ω_0 by a chopper. The sample has optical absorption coefficient $\beta_s(\lambda)$ and is in intimate contact with a pyroelectric transducer thin film of thickness L_p. The optical absorption coefficient and pyroelectric coefficient of the detector are $\beta_p(\lambda)$ and p, respectively. The sample/transducer system is supported by a transparent backing material of a thickness which is large compared to L_s or L_p. The photopyroelectric cell is open and the incident light is assumed to illuminate the sample surface uniformly. Light absorption by the sample/transducer system and nonradiative energy conversion to heat increases the temperature of the pyroelectric thin film. This temperature increase results in a potential difference between the upper and lower surfaces of the transducer due to the pyroelectric effect. This voltage $V[\omega_0, \beta_s(\lambda)]$ amounts to an electrical signal, which is measured in the external circuit through the connection of Ohmic leads to the pyroelectric as shown in Fig. 1.

The charge accumulated in the pyroelectric, due to a change ΔT in temperature is given by[8]

$$Q = p\Delta T \tag{1}$$

For a thin pyroelectric film of thickness L_p, exposed to a sinusoidally varying temperature field, the average charge induced due to the pyroelectric effect is

$$\langle Q\rangle = p\langle \Delta T\rangle = (p/L_p)\mathrm{Re}\left(\int_{\text{Thickness of pyroelectric film}} T(x)e^{i\omega_0 t}dx\right),$$

$$= (p/L_p)\mathrm{Re}\left[\left(\int_{\text{Thickness } L_p} T(x)dx\right)e^{i\omega_0 t}\right]. \tag{2}$$

The average pyroelectric voltage is given by

$$V = \langle Q\rangle/C, \tag{3}$$

where C is the capacitance per unit area of the thin film. For two parallel charged plates of thickness L_p and dielectric constant K, Eq. (3) becomes

$$V(\omega_0) = \left[\frac{pL_p\theta_p(\omega_0)}{K\epsilon_0}\right]\exp(i\omega_0 t), \tag{4}$$

where

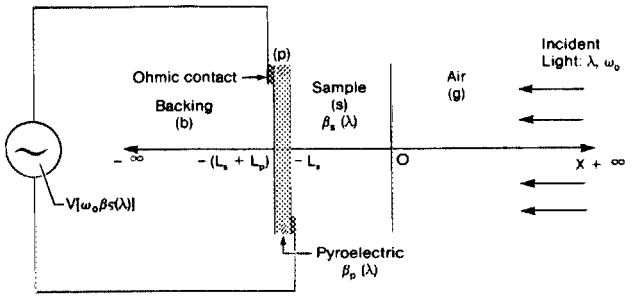

FIG. 1. One-dimensional geometry of a photopyroelectric system.

$$\theta_p(\omega_0) \equiv \frac{1}{L_p}\int_{\text{Thickness } L_p} T_p(\omega_0, x)dx, \tag{5}$$

and ϵ_0 is the permittivity constant of vacuum ($8.854\,18\times10^{-12}$ C/V m). $T_p(\omega_0, x)$ is the temperature field in the bulk of the pyroelectric, a result of heat conduction processes through the radiation absorbing solid. For the geometry of Fig. 1 the field $T_p(\omega_0, x)$ can be found from the solution of coupled, one-dimensional thermal transport equations. Allowing for the finite optical absorption coefficients β_s and β_p, and assuming negligible optical reflection and radiative heat transfer coefficients on the sample surface and pyroelectric-sample interface,[9] the appropriate heat diffusion equations have the form

$$\frac{d^2}{dx^2}T_g(\omega_0, x) - \left(\frac{i\omega_0}{\alpha_g}\right)T_g(\omega_0, x) = 0; \quad x \geqslant 0, \tag{6a}$$

$$\frac{d^2}{dx^2}T_s(\omega_0, x) - \left(\frac{i\omega_0}{\alpha_s}\right)T_s(\omega_0, x)$$
$$= -(I_0\beta_s\eta_s/2k_s)\exp(\beta_s x); \quad -L_s \leqslant x \leqslant 0, \tag{6b}$$

$$\frac{d^2}{dx^2}T_p(\omega_0, x) - \left(\frac{i\omega_0}{\alpha_p}\right)T_p(\omega_0, x)$$
$$= -(I_0\beta_p\eta_p e^{-\beta_s L_s}/2k_p)\exp[\beta_p(x + L_s)]; \quad -(L_p + L_s) \leqslant x \leqslant -L_s, \tag{6c}$$

and

$$\frac{d^2}{dx^2}T_b(\omega_0, x) - \left(\frac{i\omega_0}{\alpha_b}\right)T_b(\omega_0, x) = 0; \quad x \leqslant -(L_p + L_s). \tag{6d}$$

In Eqs. (6a)–(6d), a harmonic dependence of all temperatures on time was assumed:

$$T_j(\omega_0, x; t) = T_j(\omega_0, x)e^{i\omega_0 t}; \quad j = g, s, p, b. \tag{7}$$

The following parameters were also defined: α_j, the thermal diffusivity of $j(=g, s, p, b)$; k_j, the thermal conductivity of j; η_s and η_p, the nonradiative conversion efficiencies for the absorbing solid and pyroelectric, respectively. I_0 is the light source irradiance incident at the solid sample surface.

The Eqs. (6a)–(6d) are coupled via boundary conditions of temperature and heat flux continuity at all interfaces:

$$T_i(\omega_0, \text{ boundary}) = T_j(\omega_0, \text{ boundary}), \tag{8a}$$

$$k_i\frac{\partial}{\partial x}T_i(\omega_0, \text{ boundary}) = k_j\frac{\partial}{\partial x}T_j(\omega_0, \text{ boundary}). \tag{8b}$$

The complete complex solutions to Eqs. (6) are

$$T_g(\omega_0, x) = C_1\exp(-\sigma_g x), \tag{9a}$$

$$T_s(\omega_0, x) = \left(\frac{I_0\beta_s\eta_s}{2k_s(\sigma_s^2 - \beta_s^2)}\right)\exp(\beta_s x) + C_2\exp(\sigma_s x) + C_3\exp(-\sigma_s x), \tag{9b}$$

$$T_p(\omega_0, x) = \left[\frac{I_0\beta_p\eta_p\exp(-\beta_s L_s)}{2k_p(\sigma_p^2 - \beta_p^2)}\right]\exp[\beta_p(x + L_s)] + C_4\exp(\sigma_p x) + C_5\exp(-\sigma_p x), \tag{9c}$$

and

$$T_b(\omega_0, x) = C_6\exp(\sigma_b x), \tag{9d}$$

where

$$\sigma_j \equiv (1+i)a_j \quad \text{and} \quad a_j = (\omega_0/2\alpha_j)^{1/2}. \tag{10}$$

The quantity of interest is the function for the temperature field in the pyroelectric, $T_p(\omega_0, x)$. The constant coefficients C_4 and C_5 in expression (9c) can be determined from the boundary conditions (8a), (8b), which yield the following matrix equation:

$$\begin{bmatrix} 1 & -1 & -1 & 0 & 0 & 0 \\ 1 & b_{sg} & -b_{sg} & 0 & 0 & 0 \\ 0 & X^{-1} & X & -Y^{-1} & -Y & 0 \\ 0 & X^{-1} & -X & -b_{ps}Y^{-1} & b_{ps}Y & 0 \\ 0 & 0 & 0 & Z^{-1} & Z & -W^{-1} \\ 0 & 0 & 0 & Z^{-1} & -Z & -b_{bp}W^{-1} \end{bmatrix} \begin{bmatrix} C_1 \\ C_2 \\ C_3 \\ C_4 \\ C_5 \\ C_6 \end{bmatrix} = \begin{bmatrix} -E \\ b_{sg}r_s E \\ Ee^{-\beta_s L_s} - Fe^{-\beta_p L_s} \\ Er_s e^{-\beta_s L_s} - Fb_{ps}r_p e^{-\beta_p L_s} \\ Fe^{-\beta_p(L_s+L_p)} \\ Fr_p e^{-\beta_p(L_s+L_p)} \end{bmatrix},$$

or

$$\mathfrak{M}\mathfrak{C} = \mathfrak{Q}, \tag{11}$$

where

$$b_{mn} \equiv k_m a_m / k_n a_n; \quad r_j \equiv \beta_j/\sigma_j, \tag{12}$$

$$X \equiv \exp(\sigma_s L_s), \tag{13}$$

$$Y \equiv \exp(\sigma_p L_s), \tag{14}$$

$$Z \equiv \exp[\sigma_p(L_s+L_p)], \tag{15}$$

$$W \equiv \exp[\sigma_b(L_s+L_p)], \tag{16}$$

$$E \equiv I_0\beta_s\eta_s/2k_s(\beta_s^2-\sigma_s^2), \tag{17}$$

$$F \equiv \{I_0\beta_p\eta_p \exp[-(\beta_s-\beta_p)L_s]\} \div 2k_p(\beta_p^2-\sigma_p^2). \tag{18}$$

The solution of the matrix equation (11) is

$$\mathfrak{C} = \mathfrak{M}^{-1}\mathfrak{Q} \tag{19}$$

with $(\mathfrak{M}^{-1})_{ij} = (\text{adj}\,\mathfrak{M})_{ij}/(\det \mathfrak{M})$,

so that

$$C_4 = \frac{1}{\det \mathfrak{M}} \sum_{i=1}^{6} (\text{adj}\,\mathfrak{M})_{i,4}(\mathfrak{Q})_i, \tag{20}$$

and

$$C_5 = \frac{1}{\det \mathfrak{M}} \sum_{i=1}^{6} (\text{adj}\,\mathfrak{M})_{i,5}(\mathfrak{Q})_i. \tag{21}$$

Using Eq. (9c) in the expression for the average temperature $\theta_p(\omega_0)$ of the pyroelectric thin film, Eq. (5), we obtain

$$\theta_p(\omega_0) = \frac{1}{L_p}\int_{-(L_s+L_p)}^{-L_s} T_p(\omega_0, x)\,dx,$$

$$= \frac{1}{L_p}\left\{\frac{1}{\sigma_p}[(1-e^{-\sigma_p L_p})e^{-\sigma_p L_s}C_4 + (e^{\sigma_p L_p}-1)e^{\sigma_p L_s}C_5] - (F/\beta_p)(1-e^{-\beta_p L_p})e^{-\beta_p L_s}\right\}. \tag{22}$$

Insertion of Eqs. (20) and (21) in Eq. (22) gives the following general expression for $\theta_p(\omega_0)$, after a considerable amount of algebraic manipulation:

$$\begin{aligned}
\theta_p(\omega_0) = {} & \left(\frac{I_0}{2\sigma_p L_p}\right)\left\{\left(\frac{\beta_s\eta_s}{k_s(\beta_s^2-\sigma_s^2)}\right)(\{[\exp(\sigma_p L_p)-1](b_{bp}+1) - [1-\exp(-\sigma_p L_p)](b_{bp}-1)\}\right. \\
& \times\{2(b_{sg}r_s+1) - [(r_s+1)(b_{sg}+1)\exp(\sigma_s L_s) + (r_s-1)(b_{sg}-1)\exp(-\sigma_s L_s)]\exp(-\beta_s L_s)\}) \\
& + \left(\frac{\beta_p\eta_p\exp(-\beta_s L_s)}{k_p(\beta_p^2-\sigma_p^2)}\right)\{[\{\{[\exp(\sigma_p L_p)-1](b_{bp}+1) - [1-\exp(-\sigma_p L_p)](b_{bp}-1)\}(b_{ps}r_p+1) \\
& + \{[\exp(\sigma_p L_p)-1](b_{ps}+1) + [1-\exp(-\sigma_p L_p)](b_{ps}-1)\}(b_{bp}-r_p)\exp(-\beta_p L_p)) \\
& - r_p^{-1}\{(b_{bp}+1)(b_{ps}+1)\exp(\sigma_p L_p) \\
& + (b_{bp}-1)(b_{ps}-1)\exp(-\sigma_p L_p)\}[1-\exp(-\beta_p L_p)]](b_{sg}+1)\exp(\sigma_s L_s) + [(\{[\exp(\sigma_p L_p)-1](b_{bp}+1) \\
& - [1-\exp(-\sigma_p L_p)](b_{bp}-1)\}(b_{ps}r_p-1) + \{[\exp(\sigma_p L_p)-1](b_{ps}-1) \\
& + [1-\exp(-\sigma_p L_p)](b_{ps}+1)\}(b_{bp}-r_p)\exp(-\beta_p L_p)) \\
& - r_p^{-1}\{(b_{bp}+1)(b_{ps}-1)\exp(\sigma_p L_p) + (b_{bp}-1)(b_{ps}+1)\exp(-\sigma_p L_p)\}[1-\exp(-\beta_p L_p)]] \\
& \left.\times(b_{sg}-1)\exp(-\sigma_s L_s)\}\right\} \\
& \div\{(b_{sg}+1)[(b_{bp}+1)(b_{ps}+1)\exp(\sigma_p L_p) + (b_{bp}-1)(b_{ps}-1)\exp(-\sigma_p L_p)]\exp(\sigma_s L_s) \\
& + (b_{sg}-1)[(b_{bp}+1)(b_{ps}-1)\exp(\sigma_p L_p) + (b_{bp}-1)(b_{ps}+1)\exp(-\sigma_p L_p)]\exp(-\sigma_s L_s)).
\end{aligned} \tag{23}$$

Further substitution of Eq. (23) into Eq. (4) gives the desired expression for the complex photopyroelectric voltage as a function of the modulation frequency of light, optical, thermal, and geometric parameters of the sample/pyroelectric system. The complex quantity $V(\omega_0)$ can be most conveniently evaluated by writing its components in polar coordinate notation, thus introducing amplitude and phase factors:

$$V(\omega_0) = |V(\omega_0)| \exp\{i[\omega_0 t - \Phi(\omega_0)]\}. \tag{24}$$

In Eq. (24), the following polar coordinate definitions have been made for the general case of Eq. (23):

(i) Photopyroelectric voltage amplitude

$$|V(\omega_0)| = \frac{p|M(\omega_0)|}{\sqrt{2}K\epsilon_0 a_p |S_4(\omega_0)|}, \tag{25a}$$

(ii) Phase $\Phi(\omega_0) = \frac{\pi}{4} + \psi_4(\omega_0) - q(\omega_0)$. (25b)

The various quantities appearing in Eqs. (25a) and (25b) have been defined in the Appendix.

III. SPECIAL CASES

Equation (23) demonstrates explicitly that the thickness-averaged photopyroelectric signal is a function of both the optical and thermal parameters of the solid sample under investigation. The complicated dependence of the signal on the sample-related parameters, however, renders any physical insight into Eq. (23) very difficult in the general case. Therefore, we are considering several special cases in this section, according to the optical opacity or transparency of the sample. The classification scheme used here was adopted from Rosencwaig and Gersho.[14] Specifically, all cases evaluated below have been classified according to the relative magnitudes of three characteristic lengths in the solid and the pyroelectric, namely, (i) thickness L_s or L_p; (ii) optical absorption depth μ_{β_s} or μ_{β_p}, defined as

$$\mu_{\beta_j} \equiv \beta_j^{-1}, \tag{26}$$

and (iii) thermal diffusion length μ_s or μ_p, defined from Eq. (10):

$$\mu_j \equiv a_j^{-1} = (2\alpha_j/\omega_0)^{1/2} \tag{27}$$

For the special cases considered below, the thin pyroelectric film detector was assumed to possess a high optical absorption coefficient for all light wavelengths of interest. This assumption is well founded for Kynar™ PVF_2 films coated with nickel and exposed to near UV-VIS radiation.[9] For the purposes of the present theoretical treatment, transducer opacity conveniently eliminates undue complications of interpretation from undesirable superposition of the optical characteristics of the detector on the spectral features of the sample. It should be mentioned that transducer opacity corresponds to photopyroelectric saturation with respect to the pyroelectric film. For the special cases of the photopyroelectric signal discussed below, the time-dependent factor $\exp(i\omega_0 t)$ in Eq. (4) has been omitted, as it does not affect the amplitude or the phase lag of the complex envelope of the signal.

A. Optically opaque and thermally thick pyroelectric

This case is likely to occur experimentally at high chopping frequencies ω_0 and/or for thick transducers. In this limit $\mu_{\beta_p} \ll L_p$, $\mu_p < L_p$, and $\mu_{\beta_p} < \mu_p$. In Eq. (23) we set

$$\exp(-\beta_p L_p) \cong 0, \quad \exp(-\sigma_p L_p) \cong 0, \quad \text{and} \quad |r_p| > 1.$$

Then

$$\begin{aligned} V(\omega_0,\beta_s) &= \frac{pI_0}{2k\epsilon_0}\left[\left(\frac{\beta_s\eta_s}{k_s(\beta_s^2-\sigma_s^2)\sigma_p}\right)\{2(b_{sg}r_s+1) - [(r_s+1)(b_{sg}+1)\exp(\sigma_s L_s) + (r_s-1)(b_{sg}-1)\exp(-\sigma_s L_s)]\exp(-\beta_s L_s)\}\right. \\ &\left. + \left(\frac{n_p\exp(-\beta_s L_s)}{k_p\beta_p\sigma_p}\right)\{(b_{sg}+1)(b_{ps}r_p+1)\exp(\sigma_s L_s) + (b_{sg}-1)(b_{ps}r_p-1)\exp(-\sigma_s L_s)\}\right] \\ &\div [(b_{sg}+1)(b_{ps}+1)\exp(\sigma_s L_s) + (b_{sg}-1)(b_{ps}-1)\exp(-\sigma_s L_s)]. \end{aligned} \tag{28}$$

1. Optically opaque sample ($\mu_{\beta_s} \ll L_s$)

In Eq. (28) set $\exp(-\beta_s L_s) \cong 0$.

Case A.1 (a): Thermally thin sample ($\mu_s \gg L_s$, $\mu_s \gg \mu_{\beta_s}$). In Eq. (28) we set $\exp(\pm\sigma_s L_s) \cong 1$, and $|r_s| \gg 1$. The result is

$$V(\omega_0) = A\left(\frac{\eta_s}{\sigma_p(k_p\sigma_p + k_g\sigma_g)}\right), \tag{29}$$

$$= A\left(\frac{\eta_s\alpha_p}{k_p(1+b_{gp})\omega_0}\right)\exp(-i\pi/2), \tag{30}$$

where

$$A \equiv pI_0/2k\epsilon_0. \tag{31}$$

Equations (29) and (30) show that the photopyroelectric voltage is independent of β_s. This behavior can be termed *photopyroelectric saturation*. The signal depends on thermal properties of both the gas and the pyroelectric, it varies with chopping frequency as ω_0^{-1}, and its phase lags by 90° that of the light intensity modulating device (the chopper).

Case A.1(b): Thermally thick sample ($\mu_s < L_s$; $\mu_s > \mu_{\beta_s}$). In Eq. (28) set $\exp(-\sigma_s L_s) = 0$, and $|r_s| > 1$. Assuming that $|r_s| > b_{gs}$, a reasonable assumption for g = gas (e.g., air), Eq. (28) reduces to

$$V(\omega_0) = A\left(\frac{\eta_s\exp(-\sigma_s L_s)}{\sigma_p(k_p\sigma_p + k_s\sigma_s)}\right), \tag{32}$$

$$= A\left(\frac{\eta_s\alpha_p}{k_p(1+b_{sp})\omega_0}\right)\exp\left[-\left(\frac{\omega_0}{2\alpha_s}\right)^{1/2}L_s\right] \times \exp\left\{-i\left[\frac{\pi}{2} + \left(\frac{\omega_0}{2\alpha_s}\right)^{1/2}L_s\right]\right\}. \tag{33}$$

In this limit, the photopyroelectric signal is saturated with

respect to β_s as in the previous case. The voltage amplitude $|V(\omega_0)|$, however, is extremely small and decreases more rapidly than ω_0^{-1}, while the voltage phase lag increases with the square root of ω_0. The thermal properties of the contact gas have now been replaced with those of the solid. Equations (32) and (33) indicate that in this limit the photopyroelectric signal can be used, in principle, to determine the thickness L_s of the sample, if its thermal diffusivity α_s is known, or vice versa. However, practical difficulties may arise due to the very small magnitude of the signal.

Case A.1(c): Thermally thick sample ($\mu_s \ll L_s$, $\mu_s < \mu_{\beta_s}$). In Eq. (28) set $\exp(-\sigma_s L_s) \cong 0$, and $|r_s| < 1$. Here, two possibilities can occur: (i) $|r_s| < b_{sg} < 1$; then

$$V(\omega_0,\beta_s) = -A\left(\frac{\eta_s \beta_s b_{sg} \exp(-\sigma_s L_s)}{\sigma_p \sigma_s (k_p \sigma_p + k_s \sigma_s)}\right), \tag{34}$$

$$= A\beta_s \left(\frac{\eta_s b_{sg} \alpha_s \sqrt{\alpha_p}}{k_p (1 + b_{sp}) \omega_0^{3/2}}\right) \exp\left[-\left(\frac{\omega_0}{2\alpha_s}\right)^{1/2} L_s\right] \times \exp\left\{-i\left[\left(\frac{\omega_0}{2\alpha_s}\right)^{1/2} L_s - \frac{\pi}{4}\right]\right\} \tag{35}$$

This case can be called Thermal Transmission Spectroscopy. It is of spectroscopic interest, as the photopyroelectric voltage is out of the saturation and proportional to β_s. Optically, the sample is opaque; however, as long as $\mu_s < \mu_{\beta_s}$, the exponential tail of the heat wave generated within μ_s in the sample is communicated to the pyroelectric transducer, thus producing a signal linear in β_s and of small magnitude. In this limit the sample is optically but not photopyroelectrically opaque. Therefore, the technique can be used in this limit as a spectroscopy, yielding signal information similar to absorption spectra. The other possibility to be considered here is (ii) $b_{sg} < |r_s| < 1$; then Eq. (28) becomes

$$V(\omega_0,\beta_s) = -A\left(\frac{\eta_s \beta_s^2 \exp(-\sigma_s L_s)}{\sigma_p \sigma_s^2 (k_p \sigma_p + k_s \sigma_s)}\right), \tag{36}$$

$$= A\beta_s^2 \left(\frac{\eta_s \alpha_p \alpha_s}{k_p (1 + b_{sp}) \omega_0^2}\right) \exp\left[-\left(\frac{\omega_0}{2\alpha_s}\right)^{1/2} L_s\right] \times \exp\left[-i\left(\frac{\omega_0}{2\alpha_s}\right)^{1/2} L_s\right]. \tag{37}$$

This case is not as useful experimentally as the one above, (i). Equations (36) and (37) predict a spectral nonlinearity, i.e., $V(\omega_0,\beta_s) \propto \beta_s^2$. This dependence would tend to distort spectral information from the sample; therefore, it is regarded as undesirable.

2. Optically transparent sample ($\mu_{\beta_s} > L_s$)

In Eq. (28) set $\exp(-\beta_s L_s) \cong 1 - \beta_s L_s$.

Case A.2(a): Thermally thin sample ($\mu_s \gg L_s$; $\mu_s > \mu_{\beta_s}$). In Eq. (28) we set $\exp(\pm \sigma_s L_s) \cong 1$, and $|r_s| > 1$. This results in the following expression:

$$V(\omega_0,\beta_s) = A\left(\frac{\eta_p + (\eta_s - \eta_p)\beta_s L_s}{\sigma_p (k_p \sigma_p + k_g \sigma_g)}\right), \tag{38}$$

$$= A\left(\frac{\eta_p + (\eta_s - \eta_p)\beta_s L_s}{k_p (1 + b_{gp}) \omega_0}\right) \exp(-i\pi/2). \tag{39}$$

The photopyroelectric voltage is proportional to $\beta_s L_s$, provided that $\eta_s \neq \eta_p$. In the experimentally common case where $\eta_s \sim \eta_p \sim 1$ and $b_{gp} < 1$, the signal carries neither optical nor thermal information about the sample, and is entirely generated by direct light absorption in the pyroelectric.

Case A.2(b): Thermally thin sample ($\mu_s > L_s$; $\mu_s < \mu_{\beta_s}$). In Eq. (28) we set $\exp(\pm \sigma_s L_s) \cong 1 \pm \sigma_s L_s$; and $|r_s| < 1$. Further, if we assume (i) $|r_s| \gg |\sigma_s L_s|$, i.e., $\mu_s^2 > \mu_{\beta_s} L_s$, Eq. (28) reduces to

$$V(\omega_0,\beta_s) = A\left(\frac{\eta_p + (\eta_s - \eta_p)\beta_s L_s}{k_p \sigma_p^2}\right), \tag{40}$$

$$= A\alpha_p \left(\frac{\eta_p + (\eta_s - \eta_p)\beta_s L_s}{k_p \omega_0}\right) \exp(-i\pi/2). \tag{41}$$

This case is similar to A.2(a) in that, for $\eta_p \sim \eta_s \sim 1$, no optical or thermal information about the sample is obtained. If, however, we assume $|r_s| \ll |\sigma_s L_s|$, then

$$V(\omega_0,\beta_s) = A\left(\frac{(\eta_p + \eta_s \beta_s L_s)(1 - \beta_s L_s)}{k_p \sigma_p^2}\right), \tag{42}$$

$$= A\alpha_p \left[\frac{(\eta_p + \eta_s \beta_s L_s)(1 - \beta_s L_s)}{k_p \omega_0}\right] \exp(-i\pi/2). \tag{43}$$

Here, if $\eta_p \sim \eta_s \sim 1$, the photopyroelectric voltage will be proportional to $1 - (\beta_s L_s)^2$, with a ω_0^{-1} frequency dependence. This limit is nonlinear in β_s and the spectral information from the system will be similar to distorted transmission spectra.

Case A.2(c): Thermally thick sample ($\mu_s < L_s$; $\mu_s \ll \mu_{\beta_s}$). The approximations in Eq. (28) are: $\exp(-\sigma_s L_s) \cong 0$, and $|r_s| \ll 1$. The photopyroelectric voltage then is

$$V(\omega_0,\beta_s) = A\left(\frac{\eta_p (1 - \beta_s L_s)}{\sigma_p (k_p \sigma_p + k_s \sigma_s)}\right), \tag{44}$$

$$= A(1 - \beta_s L_s)\left(\frac{\eta_p}{k_p (1 + b_{sp}) \omega_0}\right) \exp(-i\pi/2). \tag{45}$$

In this limit the technique is equivalent to optical transmission spectroscopy. It is of great experimental interest, because the photopyroelectric voltage amplitude is proportional to $1 - \beta_s L_s$. Therefore, the technique can yield signal information similar to a transmission spectrum. In this case, unlike case A.1(c;i), a photon counter could also be used in place of the pyroelectric substrate, if the experimental geometry favored such a device, or if a better signal to noise ratio could thereby be achieved. It must be emphasized that cases A.1(c;i), and A.2(c) are the only spectroscopically important cases, which give *direct* and undistorted information about the optical absorption coefficient of the sample material, as the result of thermal and optical transmission, respectively.

B. Optically opaque and thermally thin pyroelectric

This case is likely to occur at low chopping frequencies ω_0 and/or very thin pyroelectric films. Under this condition: $\mu_{\beta_p} \gg L_p$, and $\mu_p \gg \mu_{\beta_p}$. Upon setting $\exp(-\beta_p L_p) \cong 0$, $\exp(\pm \sigma_p L_p) \cong 1 \pm \sigma_p L_p$, $|r_p| \gg 1$ in Eq. (23), we obtain the expression

$$V(\omega_0,\beta_s) = A\left[\left(\frac{\beta_s\eta_s L_p}{k_s(\beta_s^2-\sigma_s^2)}\right)\{2(b_{sg}r_s+1)-[(r_s+1)(b_{sg}+1)\exp(\sigma_s L_s)+(r_s+1)(b_{sg}-1)\exp(-\sigma_s L_s)]\exp(-\beta_s L_s)\}\right.$$

$$+\left(\frac{\eta_p\exp(-\beta_s L_s)}{k_p\beta_p\sigma_p}\right)\{(b_{sg}+1)[(b_{ps}r_p+1)\sigma_p L_p - r_p^{-1}\{(b_{bs}+1)+(b_{ps}+b_{bp})\sigma_p L_p\}]\exp(\sigma_s L_s)$$

$$\left.+(b_{sg}-1)[(b_{ps}r_p-1)\sigma_p L_p - r_p^{-1}\{(b_{bs}-1)+(b_{ps}-b_{bp})\sigma_p L_p]\exp(-\sigma_s L_s)\}\right]$$

$$\div\{(b_{sg}+1)[(b_{bs}+1)+(b_{ps}+b_{bp})\sigma_p L_p]\exp(\sigma_s L_s)+(b_{sg}-1)[(b_{bs}-1)+(b_{ps}-b_{bp})\sigma_p L_p]\exp(-\sigma_s L_s)\}. \quad (46)$$

There are six special limits of Eq. (46), involving relationships between μ_s, μ_{β_s}, and L_s identical to those examined in cases A.1 and A.2, above. For each limit in the case of thermally thin pyroelectric transducer, the simplified expression for $V(\omega_0,\beta_s)$ which results from Eq. (46) is structurally similar to the respective expression in the case of the thermally thick detector examined previously, with the following substitutions:

Thermally thick pyroelectric		*Thermally thin pyroelectric*
(a) $1/\sigma_p$	$\rightarrow$	L_p,
(b) $k_p\sigma_p$	$\rightarrow$	$k_b\sigma_b$.

(47)

According to substitutions (47), the cases of spectroscopic interest in the limit of thermally thin pyroelectric are

(i) Case B.1 (c; i): Thermal transmission mode.

$$V(\omega_0,\beta_s) = -A\left(\frac{\eta_s\beta_s L_p b_{sg}\exp(-\sigma_s L_s)}{\sigma_s(k_b\sigma_b+k_s\sigma_s)}\right), \quad (48)$$

and

(ii) Case B.2(c): Optical transmission mode.

$$V(\omega_0,\beta_s) = A\left(\frac{\eta_p L_p(1-\beta_s L_s)}{k_b\sigma_b+k_s\sigma_s}\right). \quad (49)$$

The frequency dependence of the photopyroelectric voltage in all cases (B) is consistently a factor $\omega_0^{-1/2}$ lower than all cases (A).

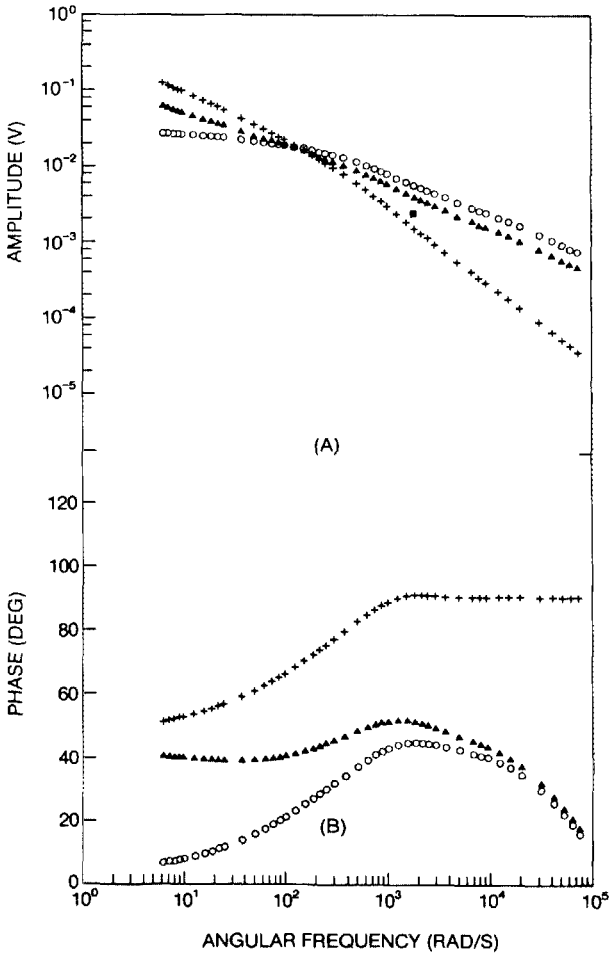

FIG. 2. Photopyroelectric frequency response of solids with high thermal conductivity on an optically opaque pyroelectric film: (A) amplitude, and (B) phase: $\beta_p = 10\ \mathrm{m}^{-1}$, $b_{ps} = 0$. ○: $\beta_s = 100\ \mathrm{m}^{-1}$; ▲: $\beta_s = 1\times10^4\ \mathrm{m}^{-1}$; +: $\beta_s = 1\times10^6\ \mathrm{m}^{-1}$.

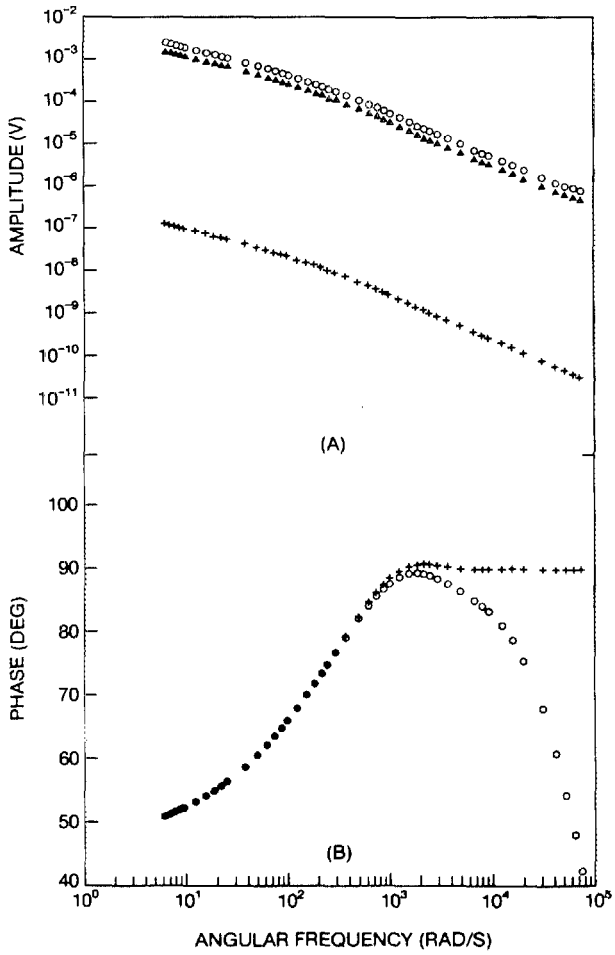

FIG. 3. Photopyroelectric frequency response of solids with low thermal conductivity on an optically opaque pyroelectric film: (A) amplitude, and (B) phase: $\beta_p = 10^6\ \mathrm{m}^{-1}$, $b_{ps} = 10^3$. ○: $\beta_s = 100\ \mathrm{m}^{-1}$; ▲: $\beta_s = 1\times10^4\ \mathrm{m}^{-1}$; + $\beta_s = 1\times10^6\ \mathrm{m}^{-1}$.

IV. DISCUSSION: GENERAL RESULTS OF THE THEORY

The full expression for the film-thickness-averaged photopyroelectric voltage, Eqs. (4) and (23) combined, was evaluated numerically using the polar coordinate notation of Eqs. (25a) and (25b) for the amplitude $|V(\omega_0)|$ and phase $\Phi(\omega_0)$ of the signal. The following numerical values were used for these calculations: $I_0 = 1$ W/m^2, $p = 3\times10^{-5}$ C/m^2 °K (Ref. 13), $K = 12$ (Ref. 13), $\epsilon_0 = 8.854\times10^{-12}$ C/V m, $L_p = 28$ μm (Ref. 13) $\alpha_p = 5.4\times10^{-8}$ m^2/sec (Ref. 13), $k_p = 0.13$ W/m °K (Ref. 13), $k_g = 2.38\times10^{-2}$ W/m °K, $\alpha_g = 1.9\times10^{-5}$ m^2/sec (g = air), and $L_s = 50$ μm. All other parameters were allowed to vary. Fig. 2 shows the photopyroelectric frequency response of a solid which is a very good thermal conductor ($b_{ps} = 0$), on an optically opaque pyroelectric ($\beta_p = 10^6$ m^{-1}). The optical absorption coefficient β_s appears as a parameter. The amplitude plot exhibits a crossover region around $\omega_0 = 100$ rad/sec. This behavior can be explained by the fact that in the optically opaque solid ($\beta_s = 10^6$ m^{-1}) heat is generated following absorption very close to the surface. This heat can be communicated to the underlying pyroelectric film as long as the thermal diffusion length μ_s is larger than the thickness L_s. At high frequencies the solid becomes thermally thick and the signal drops very rapidly, as both optical and thermal communication with the pyroelectric diminishes. In the case of a transparent solid, however, a portion of the heat that activates the transducer is generated within the pyroelectric itself via direct light absorption. This portion becomes predominant at high frequencies, the signal exceeds that due to the opaque solid case, and the crossover occurs. Meanwhile, no crossover is observed in the phase plot, with the phase from the opaque sample saturating at 90°, in agreement with case A.1(a). The behavior described in Fig. 2 is consistent, at least qualitatively, with experimental observations by Mandelis.[12] The crossover phenomenon appears to be responsible for the spectral feature inversions presented in that work.

Figure 3 shows frequency response curves similar to those of Fig. 2, for a solid which is a poor thermal conductor ($b_{ps} = 10^3$). No crossover region is shown within the frequency range of interest, because no transition from primarily sample-related optical absorption to pyroelectric-dominated absorption occurs. The registered signal response is essentially solely due to direct absorption by the pyroelectric, with amplitude curve slopes resembling those of Fig. 2(a) due to transparent and semitransparent ($\beta_s = 10^2$ and 10^4 m^{-1}) solids. In Fig. 3(b), it is interesting to note the overlap of the phase curves for $\beta_s = 10^2$ and 10^4 m^{-1}, compared to the well-resolved, corresponding amplitude curves of Fig. 3(a).

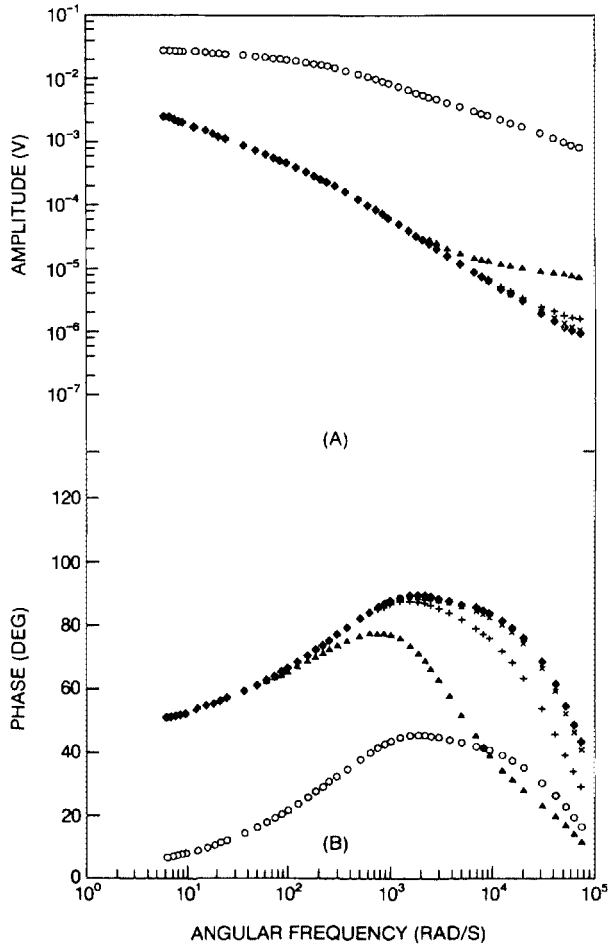

FIG. 4. Photopyroelectric frequency response of optically transparent solids: (A) amplitude, and (B) phase: $\beta_p = 10^6$ m^{-1}, $\beta_s = 100$ m^{-1}. ○: $b_{ps} = 0$; ▲: $b_{ps} = 0.1$; +: $b_{ps} = 1.0$; ×: $b_{ps} = 10$; ◆: $b_{ps} = 10^3$.

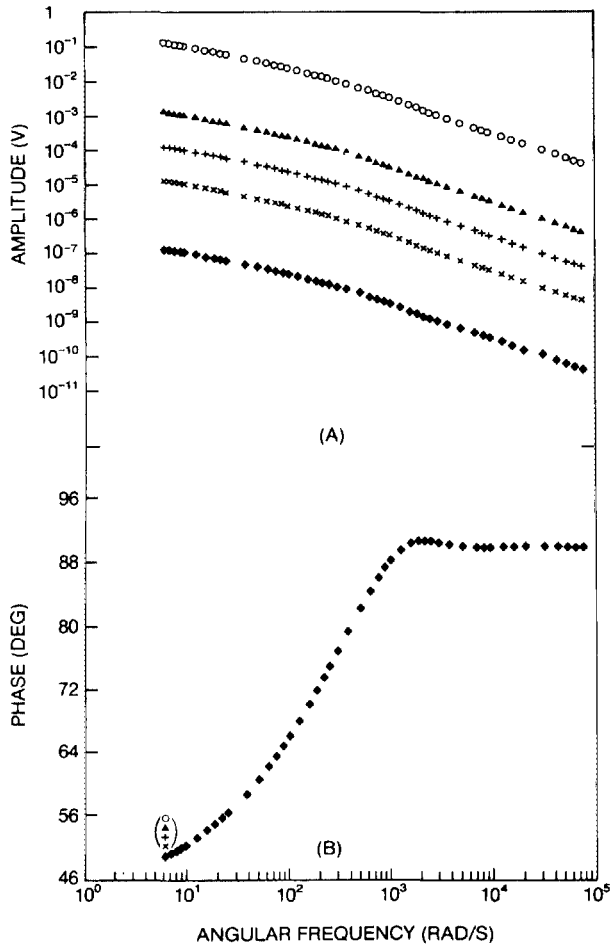

FIG. 5. Photopyroelectric frequency response of optically opaque solids: (A) amplitude, and (B) phase: $\beta_p = \beta_s = 10^6$ m^{-1}. ○: $b_{ps} = 0$; ▲: $b_{ps} = 0.1$; +: $b_{ps} = 1.0$; ×: $b_{ps} = 10$; ◆: $b_{ps} = 10^3$.

The effects of the thermal coupling coefficient b_{ps} between the pyroelectric and the sample on the photopyroelectric signal are shown in Figs. 4 and 5. Figure 4 is the frequency response of a transparent solid on an optically opaque pyroelectric, with the thermal diffusivity of the solid as a parameter. Signals are higher for good thermal conductors, as expected. As α_s decreases, so does the contribution of the sample-generated thermal energy to the photopyroelectric signal. For $b_{ps} \gtrsim 10$, the signals are essentially generated by the pyroelectric itself, with a substantial contribution from the sample at high frequencies only. At these frequencies, the thermal diffusion length μ_s has moved into the bulk of the sample, whose thermal contribution is now significant. In the case of Fig. 4, the phase appears to be a somewhat more sensitive measure of the importance of interplay between sample- and pyroelectric-generated thermal energy contributions to the signal. Figure 5 is parametrically similar to Fig. 4 for an optically opaque solid. Here, only light absorbed by the sample generates any photopyroelectric signal, and the amplitude curves are rigidly shifted with respect to each other, depending on α_s, i.e., the fraction of the total thermal energy that reaches the transducer within one modulation period. The phase, Fig. 5(b), does not depend on the absolute magnitude of the signal, being the ratio of the quadrature and in-phase components. Therefore, it does not vary with rigid amplitude translations.

Figure 6 shows the photopyroelectric dependence on the absorption coefficient $\beta(\lambda)$ of the solid, which is modelled as a family of Gaussian line shape absorption bands centered at 500 nm with linewidths of 0.1 eV. Both amplitude and phase responses exhibit saturation at large values of β_s ($\gtrsim 5\times 10^5$ m^{-1}), and become essentially independent of β_s for small values of that parameter ($< 10^3$ m^{-1}). These can be considered to be the useful upper and lower limits of β_s, between which the photopyroelectric effect can be utilized as a spectroscopic technique. It should be noticed that the phase correlates with the amplitude at $f = 5$ Hz.

Figure 7 shows the spectral response to the Gaussian of Fig. 6, with the chopping frequency as a parameter. A spectral inversion of the absorption amplitude peak at higher frequencies is observed, due to the interplay in thermal energy contribution between the sample and the pyroelectric, as discussed above in conjunction with Fig. 2. No inversion occurs in the phase data, which correlates with the amplitude for $f < 20$ Hz, and anticorrelates with it for higher frequencies. These trends are entirely compatible with previous experimental observations on Ho_2O_3 hydrated powders

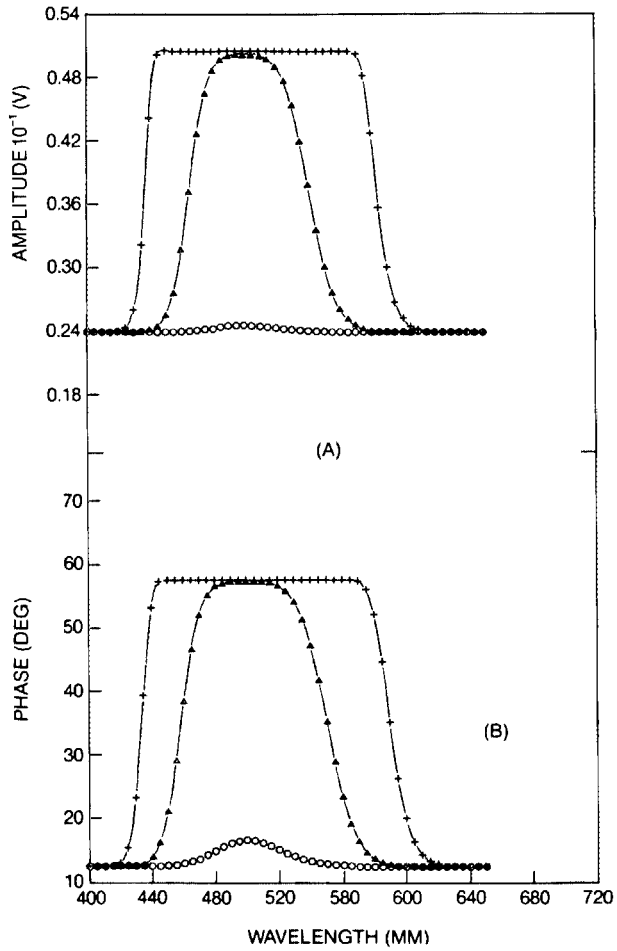

FIG. 6. Photopyroelectric spectroscopic response to a Gaussian optical absorption band:

$$\beta_s(\lambda) = \beta_0 \exp[-(12\,400^2/2)(1/\lambda - 1/500)^2],$$

with different values of β_0: (A) amplitude and (B) phase: Frequency $f = 5$ Hz, $b_{ps} = 0$. ○: $\beta_0 = 1\times 10^3$ m^{-2}; ▲: $\beta_0 = 1\times 10^5$ m^{-1}; +: $\beta_0 = 1\times 10^7$ m^{-1}.

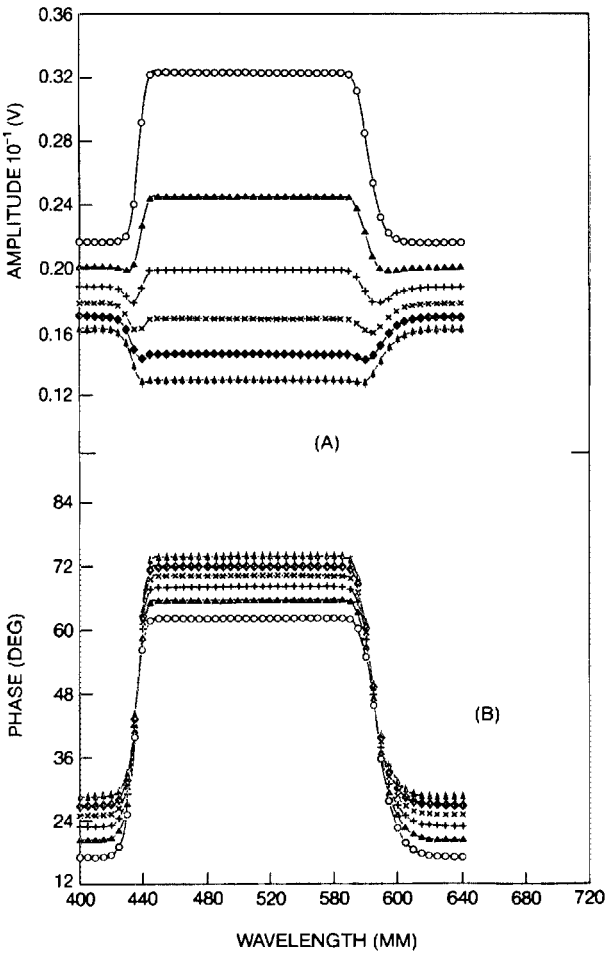

FIG. 7. Photopyroelectric spectroscopic response to the Gaussian absorption coefficient of Fig. 6 as a function of the light modulation frequency: (A) amplitude, and (B) phase: $\beta_0 = 1\times 10^7$ m^{-1}, $b_{ps} = 0$. ○: $f = 10$ Hz; ▲: $f = 15$ Hz; +: $f = 20$ Hz; ×: $f = 25$ Hz; ◆: $f = 30$ Hz; ↑: $f = 35$ Hz.

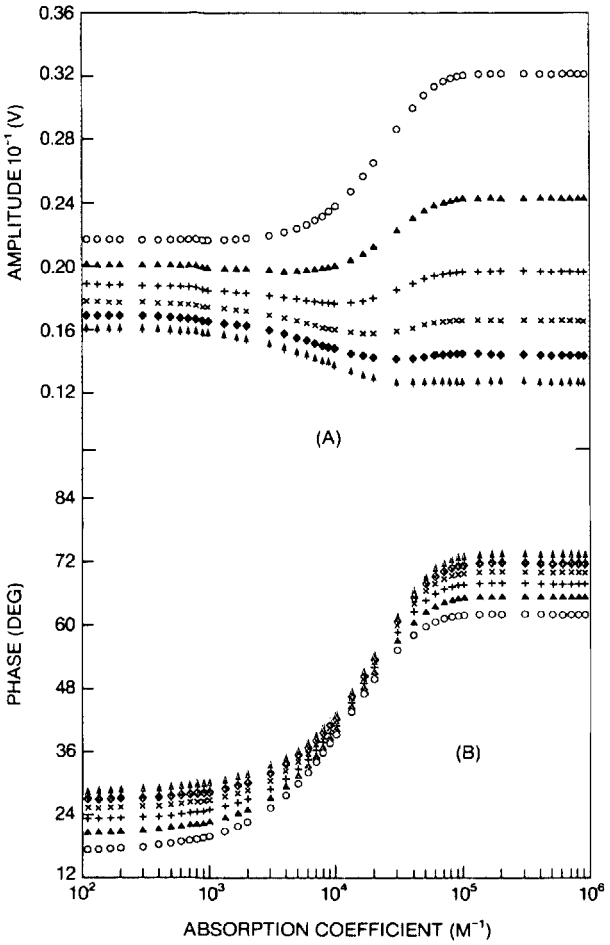

FIG. 8. Photopyroelectric signal amplitude (A), and phase (B) as a function of β_s at various modulation frequencies. Values for β_0, b_{ps}, and f are similar to those in Fig. 7, with curve symbols corresponding to the same frequency.

(Ref. 12). The figure suggests that the experimentally preferable working mode with photopyroelectric spectroscopy is using that technique with low chopping frequencies as a thermal transmission spectroscopy, in order to avoid peak inversion or splitting. The criterion for low frequencies ω_0 should be determined by the relation $\mu_s(\omega_0) \gtrsim L_s$.

Figure 8 shows the spectroscopic limits of the photopyroelectric technique in more detail than indicated in Fig. 6. The absorption spectroscopic character of the amplitude at low frequencies, and its transmission character at high frequencies, is apparent in Fig. 8(a). A comparison with the phase, Fig. 8(b), indicates that both information channels exhibit photopyroelectric saturation at the same values of β_s.

V. CONCLUSIONS

A theoretical analysis of the photopyroelectric effect has been presented. The results showed some trends familiar from other thermal wave spectroscopies, such as photoacoustic and photothermal deflection spectroscopy as well as some unique features. The usefulness of this new spectroscopic technique has been discussed from the point of view of optical absorption coefficient measurements. It was shown that, under certain conditions, inversions of the spectral features of the photopyroelectric amplitude occur, but not of the phase, in qualitative agreement with experimental evidence.[12]

The calculations showed that the photopyroelectric voltage is governed by the interplay between optical absorption in the sample and in the pyroelectric transducer itself. They suggest that it is experimentally advantageous to work with optically opaque transducers, whose flat (i.e., photopyroelectrically saturated) spectral response does not interfere with spectral measurements on the sample. Opaqueness can be achieved through coating the pyroelectric surface with metallic thin layers (e.g., nickel),[13] or black absorbing materials.[9] In the case of metallic coatings, the component of incident radiation reflected back into the overlying sample will tend to weaken the temperature gradient sampled by the transducer, provided some light can reach the pyroelectric surface (optically transparent samples). The presented special cases in this paper are, therefore, strictly applicable to optically flat pyroelectrics coated with nonhighly reflecting materials. The general expression for the photopyroelectric signal, Eq. (23), can easily incorporate the effects of the finite reflectivity R of the transducer upon multiplication by $(1-R)$ of the term proportional to $\exp(-\beta_s L_s)$.

The present theoretical considerations help establish photopyroelectric spectroscopy as a valid spectroscopic technique, to be added to the already rich arsenal of photothermal wave spectroscopies, with particularly high promise in the realm of flexible, *in-situ* nondestructive probing of samples with minimal preparation, and in applications at very high frequencies as a piezoelectric or pyroelectric thin films, such as PVF_2.[15] These features set this technique ahead of photoacoustic and photothermal spectroscopies. As a result of the latter advantage, photpyroelectric spectroscopy promises immediate applications in the study of transient phenomena through pulsed excitation in the nanosecond[16] and potentially subnanosecond time domain. The spectroscopic capability of the technique in the thermal transmission mode would be of value in electrochemical studies with the reflecting, thermally thin coating on the pyroelectric acting as the working electrode, and the photopyroelectric effect being used to measure optical and thermal processes associated with electrochemical phenomena.

ACKNOWLEDGMENTS

The authors wish to acknowledge the support of the Natural Sciences and Engineering Research Council of Canada, throughout the duration of this research. They also wish to thank the referee of the manuscript for valuable comments and suggestions.

APPENDIX

Complex quantities used in the definitions of the photopyroelectric voltage amplitude and phase, Eqs. (25a) and (25b):

$$\text{(i)}\ M(\omega_0) \equiv |M(\omega_0)| e^{iq(\omega_0)} = \left(\frac{\beta_s |S_1|}{2k_s |Z_1|}\right) \exp[i(\psi_1 - \phi_1)] + \left(\frac{\beta_p |S_5| \exp(-\beta_s L_s)}{2k_p |Z_7|}\right) \exp[i(\psi_5 - \phi_7)], \tag{A1}$$

(ii) $S_j(\omega_0) \equiv |S_j(\omega_0)| \exp[i\psi_j(\omega_0)]$, $j = 1,...,5$,

with

$$S_1(\omega_0) = 2|Z_{14}||R_1| \exp[i(\phi_{14} + \theta_1)],$$

$$= |R_1||R_2|e^{-\beta_s L_s} \exp[i(\theta_1 + \theta_2)]; \tag{A2}$$

$$S_2(\omega_0) = (b_{sg} + 1)\{|R_1||Z_8| \exp[i(\phi_8 + \theta_1)] + |R_3||Z_9|e^{-\beta_p L_p} \exp[i(\phi_9 + \theta_3)]$$

$$- (\sqrt{2}a_p/\beta_p)|R_4|[1 - \exp(-\beta_p L_p)] \exp[i(\theta_4 + \pi/4)]\}; \tag{A3}$$

$$S_3(\omega_0) = (b_{sg} - 1)\{|R_1||Z_{13}| \exp[i(\phi_{13} + \theta_1)] + |R_5||Z_9|e^{-\beta_p L_p} \exp[i(\phi_9 + \theta_5)]$$

$$- (\sqrt{2}a_p/\beta_p)|R_6|[1 - \exp(-\beta_p L_p)] \exp[i(\theta_6 + \pi/4)]\}; \tag{A4}$$

$$S_4(\omega_0) = (b_{sg} + 1)|R_4| \exp(i\theta_4) + (b_{sg} - 1)|R_6| \exp(i\theta_6); \tag{A5}$$

and

$$S_5(\omega_0) = |S_2||Z_5| \exp[i(\psi_2 + \phi_5)] + |S_3||Z_{11}| \exp[i(\psi_3 + \phi_{11})]. \tag{A6}$$

(iii) The complex quantities R_j, whose amplitudes and phases appear in Eqs. (A1)–(A5) above, are defined by

$R_j(\omega_0) \equiv |R_j(\omega_0)| \exp[i\theta_j(\omega_0)]$; $j = 1,...,6$,

with

$$R_1(\omega_0) = (b_{bp} + 1)Z_2 - (b_{bp} - 1)Z_3; \tag{A7}$$

$$R_2(\omega_0) = (b_{sg} + 1)Z_4Z_5 + (b_{sg} - 1)Z_6Z_{11}; \tag{A8}$$

$$R_3(\omega_0) = (b_{ps} + 1)Z_2 + (b_{ps} - 1)Z_3; \tag{A9}$$

$$R_4(\omega_0) = (b_{bp} + 1)(b_{ps} + 1)Z_{10} + (b_{bp} - 1)(b_{ps} - 1)Z_{12}; \tag{A10}$$

$$R_5(\omega_0) = (b_{ps} - 1)Z_2 + (b_{ps} + 1)Z_3, \tag{A11}$$

and

$$R_6(\omega_0) = (b_{pb} + 1)(b_{ps} - 1)Z_{10} + (b_{bp} - 1)(b_{ps} + 1)Z_{12}. \tag{A12}$$

(iv) The complex quantities Z_j, whose amplitudes and phases appear in Eqs. (A1)–(A12), are defined by

$Z_j(\omega_0) \equiv |Z_j(\omega_0)| \exp[i\phi_j(\omega_0)]$; $j = 1,...,14$,

with

$$Z_1(\omega_0) = \beta_s^2 - \sigma_s^2; \tag{A13}$$

$$Z_2(\omega_0) = \exp(\sigma_p L_p) - 1; \tag{A14}$$

$$Z_3(\omega_0) = 1 - \exp(-\sigma_p L_p); \tag{A15}$$

$$Z_4(\omega_0) = r_s + 1; \tag{A16}$$

$$Z_5(\omega_0) = \exp(\sigma_s L_s); \tag{A17}$$

$$Z_6(\omega_0) = r_s - 1; \tag{A18}$$

$$Z_7(\omega_0) = \beta_p^2 - \sigma_p^2; \tag{A19}$$

$$Z_8(\omega_0) = b_{ps} r_p + 1; \tag{A20}$$

$$Z_9(\omega_0) = b_{bp} - r_p, \tag{A21}$$

$$Z_{10}(\omega_0) = \exp(\sigma_p L_p); \tag{A22}$$

$$Z_{11}(\omega_0) = \exp(-\sigma_s L_s); \tag{A23}$$

$$Z_{12}(\omega_0) = \exp(-\sigma_p L_p); \tag{A24}$$

$$Z_{13}(\omega_0) = b_{ps} r_p - 1, \tag{A25}$$

and

$$Z_{14}(\omega_0) = b_{sg} r_s + 1. \tag{A26}$$

[1] F. Hayashi, doctoral dissertation, Göttingen University, Göttingen, Germany, 1912.
[2] W. C. Roentgen, Ann. Phys. **45**, 737 (1914).
[3] W. Ackerman, Ann. Phys. **46**, 197 (1916).
[4] T. Yeou, C. R. Acad. Sci. **207**, 1042 (1938).
[5] A. G. Chynoweth, J. Appl. Phys. **27**, 78 (1956).
[6] H. P. Beerman, Am. Ceram. Soc. Bull. **46**, 737 (1967).
[7] E. H. Putley, *Semiconductors and Semimetals*, Vol. 5, edtied by R. K. Willardson and A. C. Beer (Academic, New York, 1970), pp. 259 et seq.
[8] B. R. Holeman, Infrared Phys. **12**, 125 (1972).
[9] W. R. Belvin and J. Geist, Appl. Opt. **13**, 1171 (1973).
[10] S. T. Liu, Ferroelectrics **10**, 83 (1976).
[11] H. Coufal, Appl. Phys. Lett. **44**, 59 (1984).
[12] A. Mandelis, Chem. Phys. Lett. **108**, 388 (1984).
[13] For instance, Kynar™ Piezo Film Technical Manual (1983), Pennwalt Corp. 900 First Ave., King of Prussia, Pennsylvania, p. 17.
[14] A. Rosencwaig and A. Gersho, J. Appl. Phys. **47**, 64 (1976).
[15] L. Bui, H. J. Shaw, and L. T. Zitelli, Electron. Lett. **12**, 393 (1976).
[16] A. C. Tam and H. Coufal, Appl. Phys. Lett. **42**, 33 (1983).